ROMANIAN JOURNAL OF INFORMATION SCIENCE AND TECHNOLOGY
Volume **27**, Number 2, 2024, 229–240

Microstructure of VO_2 Thin Films Synthesized by Pulsed Laser Deposition

Cosmin ROMANITAN[1, *], José Manuel CAICEDO[2], Razvan PASCU[1], Iuliana MIHALACHE[1], Raluca GAVRILA[1], Marius STOIAN[1], Nikolay DJOURELOV[3], and Jessica PADILLA-PANTOJA[2]

[1]National Institute for Research and Development in Microtechnologies (IMT-Bucharest), 126A Erou Iancu Nicolae Street, Voluntari 077190, Romania

[2]Catalan Institute of Nanoscience and Nanotechnology, ICN2, CSIC and The Barcelona Institute of Science and Technology (BIST), Campus UAB, 08193 Bellaterra, Barcelona. Spain

[3]Extreme Light Infrastructure-Nuclear Physics (ELI-NP), Horia Hulubei National R&D Institute for Physics and Nuclear Engineering (IFIN-HH), Magurele, Ilfov 077125, Romania

E-mails: cosmin.romanitan@imt.ro*, jose.caicedo@icn2.cat, razvan.pascu@imt.ro, iuliana.mihalache@imt.ro, raluca.gavrila@imt.ro, marius.stoian@imt.ro, nikolay.djourelov@eli-np.ro, jessica.padilla@icn2.cat

* Corresponding author

Abstract. In this paper, *pulsed laser deposition* (PLD) at low partial oxygen pressure ($\sim$ 10 mTorr) was used to obtain VO_2 thin films. During the PLD, the deposition temperature and number of pulses were varied in order to obtain a good sample crystallinity. It was showed by *atomic force microscopy* (AFM) micrographs that the mean grain size increased from $\sim$ 40 nm to $\sim$ 90 nm at a variation of the deposition temperature from 400 °C to 500 °C. Further, by increasing of both substrate temperature and number of pulses, the mean grain size increases to 220 nm. According to the Rietveld refinement of the experimental *X-ray diffraction* (XRD) pattern, within the grain size increasing, the mean crystallite size increased from 14 nm to 22 nm, as well as a decreasing of the lattice strain from 0.29% to 0.20%. These dependencies further imply a decreasing of the dislocation density of 2.3 to 0.9×10^{12} cm^{-2}. At the same time, the optical band gap decreased from 0.72 eV (400 °C) to 0.66 eV (500 °C), reaching 0.60 eV (600 °C). Further investigations performed by *X-ray photoelectron spectroscopy* (XPS) showed the vanadium oxide presence, by the spin-orbit splitting of approximately 7.5 eV between $V2p_{3/2}$ and $V2p_{1/2}$ orbitals. Finally, the electrical measurements done in the range of $250 - 370$ K reveal a close relationship between the dislocation density and the observed resistance-temperature dependence.

Key-words: Pulsed laser deposition; resistance-temperature curves; Rietveld refinement; vanadium oxide; X-ray diffraction.

1. Introduction

Vanadium oxide (VO_x) compounds give unique properties that can be further exploited for a wide range of applications, such as charge storage, photodetectors, sensors, smart windows or photocatalysis [1, 2]. Due to the multioxidation states and various crystalline structure (+2 for VO, +3 for V_2O_3, +4 for VO_2, and +5 for V_2O_5), vanadium oxide properties are strongly linked with the actual oxidation state. For example, vanadium dioxide (VO_2) demonstrates a significant change in resistance (for microbolometers) or in the transmission spectrum (for thermochromic coatings) with varying temperature. On the other hand, the layered crystal structure of vanadium pentoxide (V_2O_5) leads to the reversible lithium-ion insertion/extraction processes, becoming suitable for electrochromic coatings and charge storage devices. Moreover, vanadium trioxide (V_2O_3) has been used extensively in energy related applications due to the oxygen deficiency which provide more active sites and gives a high specific capacity [3]. *Metal-to-insulator phase transition* (MIT) is a peculiar feature in VO_x and can be achieved by variation of temperature, pressure or doping. In particular, by temperature changes can induce large changes in the structural, electronic and optical properties. During the transition, a critical temperature (T_c) can be defined for which the crystal structure undergoes from a monoclinic insulator phase to a tetragonal metallic phase. Due to the $T_c \sim 340$ K, VO_2 has been subject of intensive research in the last decades, from both a fundamental and applicative point of view. Below T_c, VO_2 exhibits a monoclinic structure with $P2_{1/c}$ space group in which the partially filled d-band is split into an unoccupied part pushed past the π^* band and the filled part of the d-band. Above the T_c, VO_2 transforms to a tetragonal (rutile) phase with the partially filled d-band located at the Fermi level and the material is metallic [4–6]. Recently, a detailed analysis using in-situ synchrotron X-ray diffraction unveiled subtle fingerprints of this complexity in the structure of epitaxial films. During the phase transition, the crystal structure progressively transforms from monoclinic ($\sim$30 °C), to a monoclinic-tetragonal mixt phase ($\sim$45 °C), and then to tetragonal phase ($\sim$60 °C) [7]. Concomitantly, with increasing the temperature from 25 °C to 70 °C, a change of resistivity of more than two orders of magnitude took place. In this regard, MIT have aroused a great interest due to the multiple applications, such as sensors, memories, ultrafast switches, thermochromic coatings or microbolometers. Unfortunately, despite of multiple practical applications, obtaining phase pure VO_2 remains still challenging because of its narrow range of stability in the VO_2 phase of V-O phase diagram [8]. Several deposition techniques have been adopted in literature to obtain high quality VO_2, such as chemical vapor deposition [9, 10], reactive magnetron sputtering, DC/RF magnetron sputtering [11, 12] or pulsed laser deposition [13–17]. In addition to other methods, PLD affords to fabricate materials by stoichiometrically transferring target material, as well as a highly directional plasma plume towards the substrate can be created [18]. Moreover, high quality VO_2 thin films or nanostructures can be easily obtained, since it can be performed under considerably high background pressure. During the growth, the partial oxygen pressure is one of the major parameters which dramatically alter the stability of VO_x due to the multivalent states of vanadium. Also, the deposition temperature plays a crucial role in the formation of different phases and polymorphs. Bukhari *et al.* reported that the gas flow rate affects the resistivity contrast between the metallic and insulator phase, the temperature ranges of transitions and the

width of hysteresis [17]. Koussi *et al.* showed that by modifying the annealing temperature, both the transition temperature and hysteresis parameters can be controlled [16].

Moreover, the phase transition characteristics are strongly linked to the nature of the deposited material, especially in terms of grain size and defects. In general, many thin films properties have been demonstrated to have an influence on the insulator-to-metal transition parameters, such as surface morphology (roughness, defects), epitaxial lattice match, grain size and nature of grain boundaries. For instance, Suh *et al.* [14] showed that the width and shape of the hysteresis cycle are determined by the competing effects of crystallinity and grain size in VO_2 thin films on Si (100). Later, Narayan & Bhosle [19] showed that the sharpness and amplitude of the MIT transition and the hysteresis upon heating and cooling are found to be a strong function of the crystal structure and averaged crystallite size [11, 10]. According to [20], the narrowing in the band gap enhances the electron-electron interaction, that further facilitates Mott transition in VO_2. Thus, it is essential to develop suitable growth procedures, capable of crystalline VO_2 synthesis, preferably without post-annealing treatments. In the meanwhile, a detailed understanding of the relationship between the growth parameters and the resulted microstructure is necessary in order to explain different optical and electrical properties.

In this paper, we start from our previous work, where the deposition of VO_2/SiO_2/Si by PLD in one-step process was optimized, without any post-thermal processes [21]. Our findings clearly indicate that the obtaining of VO_2 layers with high crystal quality (low dislocation density) need the use of high deposition temperatures. Also, our results showed that the optical band gap is affected by the dislocation density, being reported a decrease from 0.9 eV to 0.6 eV, at a decreasing of dislocation density from 3 to 0.9×10^{11} cm^{-2}. Also, the electrical measurements pointed out that the dislocations in VO_2 induce different features in the dependence of the resistance with temperature.

2. Experimental Details

2.1. Synthesis of VO_2

The samples were grown on low-resistivity Si(100)/SiO_2 (3nm) substrate from a V_2O_5 target with high purity by PLD using a KrF excimer laser (Lambda Physik COM-Pex 201, $\lambda = 248$ nm wavelength). Film growth conditions were 10 mTorr gas pressure of pure O_2, laser fluence of 1.6 J/cm^2 and target-to-substrate distance of 54 mm. The substrate temperature was modified from 400 °C to 500 °C, and then to 600 °C. The number of pulses was 3000 for the first two samples and 8500 pulses for the latter one. The cool rate was kept at 20 °C/min in each case. For these films, the repetition rate was set at 5 Hz and the resulted thicknesses according to XRR are: 90 nm (400 °C, 3000 pulses), 140 nm (500 °C, 3000 pulses) and a thicker film at (600 °C, 8500 pulses).

2.2. Characterization

The microstructure of the growth films was evaluated by X-ray diffraction using a MRD X'Pert Pro diffractometer from Malvern-Panalytical with CuKα1 radiation with wavelength, $\lambda = 0.15406$ nm. The AFM micrographs have been acquired using Ntegra Aura (Nt-MDT) equipment, operated in semicontact (intermittent-contact) mode. The diffuse reflectance spectra of the films were collected at room temperature using an integrating sphere mounted inside Cary

5000 spectrophotometer (Agilent Technology, Santa Clara, CA, USA). The *diffuse reflectance spectra* (DRS) spectra were collected from 200 nm to 1600 nm by 1 nm intervals. All spectra were baseline corrected with 100% R baseline collected over the same spectral domain using a white polytetrafluoroethylene standard sample. Further, the Tauc function was applied to the recorded DRS spectra. *X-ray photoemission spectroscopy* (XPS) spectra were recorded on a Sigma Surface Science photoelectron spectrometer equipped with a 160-mm hemispherical energy analyzer with a 1D detector (ASPECT) and using a poly-chromatic Al X-ray (with K_α= 1486.6 eV) source at 13 kV at a power of 200 W. The area of interest was 1.3×1.3 mm^2. The analysis was performed by CasaXPS software with in advance subtracting the satellites due to the K_β radiation. All spectra were fitted using a Shirley type background and a Lorentzian-Gaussian peak shape.

2.3. Electrical measurements

Current – voltage (I-V) measurements were acquired on test samples using an electrical characterization system for wide ranges of temperature. It consists of a Keithley 4200 semiconductor characterization system and a Janis closed cycle refrigerator able to cool down up to 14K and to heat up to 500K. I-V characteristics were performed on a voltage interval between -2 – 2V, with a step of 10 mV. The 250 – 370K temperature interval was chosen for investigating our fabricated samples, acquiring at each 5K step a new I-V curve. Using the above-mentioned electrical measurements, we calculated the resistance obtained at each measure temperature, from the revers of the slope. Finally, we plotted the resistance variation as a function of temperature.

2.4. Results and discussion

Figure 1a presents the AFM images of the grown samples on 2×2 μm scan size. One can observe that the microstructure of these samples consists from grains distributed uniformly on the whole investigated area.

The grain size was analyzed using the open-source software ImageJ [22]. As can be observed in Fig. 1b, the grain size is dependent by the growth conditions. At low deposition temperature of 400 °C, the grain size was evaluated at $\sim$ 40 nm. Further, by increasing the deposition temperature at 500 °C, the grain size reaches two-fold higher values (*e.g.* $\sim$ 90 nm). For the last sample, the deposition temperature was increased to 600 °C, and concomitantly the number of pulses was modified to 8500 pulses in order to achieve higher grains, as well as a thicker film. In this case, big grains with diameter above 300 nm were detected. In the following, *X-ray reflectivity* (XRR) patterns were recorded to get the thickness of the deposited layers. In Fig. 2a, one can notice the presence of the Kiessig interference fringes at 3000 pulses.

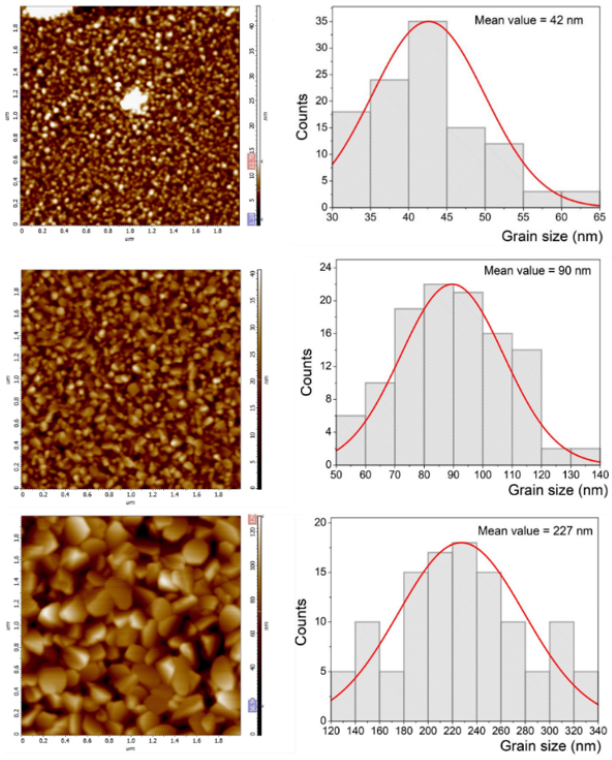

a) b)

Fig. 1. a) AFM images for the obtained samples by PLD and b) distribution of the grain size according to the ImageJ analysis on $\sim$ 100 grains.

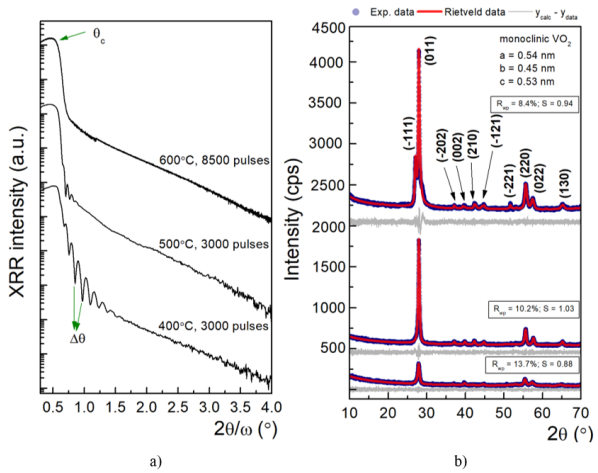

a) b)

Fig. 2. a) XRR patterns and b) GI-XRD and Rietveld data with corresponding fitting parameters R_{wp} and S on the investigated samples.

Generally, these fringes appear only in the films with small surface roughness and result from the interference between the reflected X-ray beam from the surface and the one from the interface to the substrate [23]. By analyzing the period of the fringes (labeled as $\Delta\theta$ in Fig. 2a), the film thickness, t may be determined with the following equation [24]:

$$t = {}^{\lambda}/_{\Delta\theta} \tag{1}$$

where $\lambda = 0.15406$ nm is the X-ray wavelength for CuKα1. Based on eq. (1), it was determined that the thickness $\sim$ 90 nm (400 °C, 3000 pulses), $\sim$ 140 nm (500 °C, 3000 pulses), while for the latter sample (600 °C, 8500 pulses) no interference fringes can be obtained in XRR pattern. An explanation for this could be given considering the rougher surface of this sample, as showed by AFM above. Further, in Fig. 2b are shown grazing incidence XRD spectra in the range of $2\theta = 10 - 70°$. In order to gain a deep understanding of the crystal quality for each sample, the experimental XRD patterns were fitted in the framework of the Rietveld analysis in thin films, that enables calculation of the unit cell parameters, mean crystallite size and the lattice strain. The fitting of the experimental data is performed over a broad angular range, based on information about the crystal system and lattice constants [25], [26]. In order to resolve a real structure, it requires to have a reasonable initial approximation of some parameters, *i.e.* unit cell dimensions, or coordinates of all atoms in the crystal. In the present study, the refinement was initialized starting from the initial approximation of monoclinic VO_2 from ICDD (International Centre for Diffraction data) database with a = 0.54 nm, b = 0.45 nm, c = 0.53 nm, α = 90°, β = 122.61°, γ = 90° that belongs to $P2_{1/c}$ space group. During the refinement, the background was modeled using a B-spline function, the peak shift using the shift axial displacement model, the peak shape with the pseudo-Voigt fits, while the preferred orientation by March-Dollase function. During the least squares fit of the calculated data against the experimental ones, five numerical Fig.s of merit (FOM's) were used: reliability factor (R_p), the weighted parameter (R_{wp}), the expected profile residual (R_e) and the goodness of the fit, χ^2 with S scale factor, showing the reliability of the fit. In Fig. 2b, one can observe that the experimental patterns are well-fitted with the calculated intensity (red line). According to the Rietveld data, the diffraction peaks located at: 26.92°, 27.91°, 36.93°, 39.70°, 42.36°, 44.80°, 51.35°, 55.69°, 57.50° and 65.11° can be unambiguously attributed to (–111), (011), (–202), (002), (210), (–121), (–221), (220), (022) and (031) reflections of monoclinic VO_2. Accordingly, the successful deposition of VO_2/Si, without any secondary phase is confirmed for each sample. In Table 1, are summarized the obtained results for the mean crystallite size, as well as for the lattice strain. In addition, the dislocation density calculated based on the Williamson-Smallman formula [27] is tabulated. According to the results, it is clear that the deposition temperature plays a key role in the size of the crystalline domains, since increased from $\sim$ 14 nm to $\sim$ 18 nm by increasing the temperature from 400 °C to 500 °C, keeping the same number of pulses. Further, an additional growth of the crystalline domains was achieved by increasing both the number of pulses and the deposition temperature. In this case, the mean crystallite size reached to $\sim$ 22 nm. These findings are supported by the AFM analysis, which indicated that the grain size increased from $\sim$ 40 nm, to $\sim$ 90 nm, reaching to 230 nm in the latter case.

Table 1. Mean crystallite size, lattice strain and dislocation density for the investigated samples

Sample	Mean crystallite size, τ (nm)	Lattice strain, ε (%)	Dislocation density, $\sim$ x 10^{11}, ρ (cm^{-2})
400 °C, 3000 pulses	14.1	+0.29	2.32
500 °C, 3000 pulses	17.8	+0.22	1.34
600 °C, 8500 pulses	22.1	+0.20	0.95

At the same time, within the increasing of the mean crystallite size, the lattice strain, decreased from $+0.29\%$ to $+0.20\%$, which indicate that the unit cell parameters of the deposited film are closer to the bulk VO_2. The dislocation density can be expressed as a function of the mean crystallite size and lattice strain using the following equation [27]:

$$\rho_d = \frac{\sqrt{12}\varepsilon}{\tau d_{110}} \tag{2}$$

where $d_{110} = 0.32$ nm. According to eq. (2), the samples contain different dislocation densities: $\sim 2.3 \times 10^{11}, 1.3 \times 10^{11}$ and 0.9×10^{11} cm^{-2}, as function of different growth parameters. In the following, *diffuse reflectance spectroscopy* (DRS) was employed, in order to establish the impact of the crystal quality in the band gap values. Since the band structure is very sensitive to microstructure, different microstructural features, such as grain size, defect density or lattice strain result in the changing of the band gap [28], [6]. For instance, the optical band gap has a slight red shift in the presence of small grains, which gives rise to the quantum confinement effects [29]. Also, the point defects could have localized states within the band gap, and the crystal stress may also result in the shift of band edge. Gosh *et al.*, obtained an empirical formula in ZnO thin films, which provides the empirical dependence of the band gap energy with the lattice strain [30]. It indicates that for negative strain, band gap increases, while for positive decreases. Therefore, it is expected a variation of the band gap for the investigated samples since different dislocation densities are involved. Figure 3a shows the DRS spectra of VO_2 films, for which one can note some important differences. Quantitatively, the optical absorption coefficient is related to interband transition near the band-gap and can be described as [31]:

$$\alpha h\upsilon = C(h\upsilon - E_g^{opt})^n \tag{3}$$

where υ is the frequency of the incident radiation, h is the Plank's constant, C is a constant, E_g^{opt} is the optical energy gap of the material, while the exponent n determines the type of interband electronic transition. In Fig. 3b is shown the spectral dependence of the film absorption coefficient in the plot of $(\alpha h\upsilon)^{1/n}$ versus photon energy $h\upsilon$, in the assumption that an indirect transition (n=2) is responsible for interband transitions.

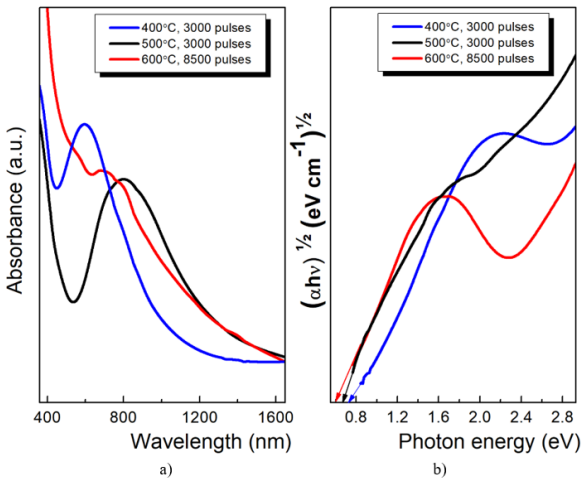

Fig. 3. a) DRS spectra for the investigated samples and b) Tauc plot in the assumption of an indirect interband transition (n = 2).

The band gap of VO_2 was determined from DRS spectra analyzed with Tauc method, through extrapolation of the linear trend observed in the spectral dependence of $(\alpha\, hv)^{1/n}$. Accordingly, it was obtained a decrease of the bandgap energy from ∼0.72 eV (400 °C) to ∼0.66 eV (500 °C) and down to ∼0.60 eV (600 °C). Luo *et al.* found that the best plot was obtained for direct allowed transitions and the optical band gap was about 0.62, 0.57 and 0.65 eV at gas pressure of 0.2, 0.3 and 0.4 Pa, respectively in VO_2 thin films prepared by reactive sputtering [10]. Goltvyanskyi *et al.* reported a band gap of 0.7 eV, 0.4 eV and 0.45 eV for low, medium and high deposition temperatures in reactive DC magnetron sputtering deposition [12]. In our case, the calculated band gap decreases with increasing the crystal quality (*i.e.* smaller dislocation density), towards the corresponding band gap of bulk VO_2 (*e.g.* ∼ 0.6 eV) [32].

Further investigations were performed to show the actual oxidation state of vanadium ions by XPS.

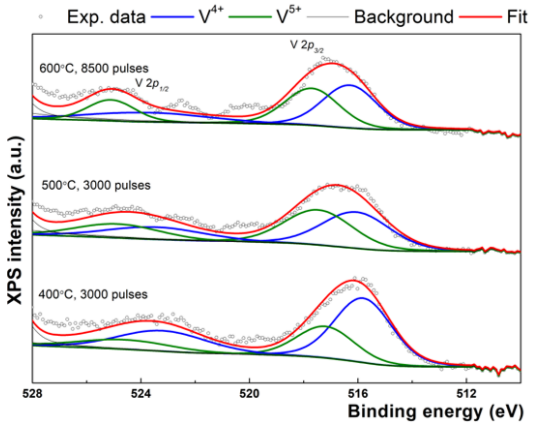

Fig. 4. Experimental XPS spectra and the corresponding fits using mixed Lorentzian–Gaussian function.

It is revealed the presence of V $2p$ doublet and the fitting were performed using a mixed Lorentzian–Gaussian function. The V $2p$ peaks show no metal V component and only high oxidation states V^{5+} and V^{4+}. The V $2p_{3/2}$ and V $2p_{1/2}$ were deconvoluted using V^{4+} (binding energy, $BE = 515.5$ and 523 eV) and V^{5+} ($BE = 517.1$ and 524.7 eV) oxidation states. Vanadium oxide presence is proved by the spin-orbit splitting of approximately 7.5 eV between V $2p_{3/2}$ and V $2p_{1/2}$ orbitals [33]. Vanadium oxidation states distribution was calculated from V $2p_{3/2}$ states. The results demonstrate that the ratio of V^{4+} (%), $V^{4+(\%)}/V^{4+(\%)+V^{5+}(\%)}$ is dependent by the growth conditions. Whereas the sample obtained at 400 °C presents a percent of $\sim 67\%$ of $^{4+}$, the samples obtained at higher temperatures have a smaller percent of V^{4+} (*e.g.* $\sim 50\%$). Thus, different band gap values could be explained considering different percent of V^{4+} and V^{5+} in the synthetized samples. According to Moatti *et al.*, a narrowing of the band gap facilitates the Mott transition in VO_2 [20].

The electrical measurements were performed on the samples to study the evolution of the normalized resistivity with temperature. In Fig. 5 is shown the normalized resistance vs. temperature data for the investigated samples on heating and cooling, in the range of 250–370 K.

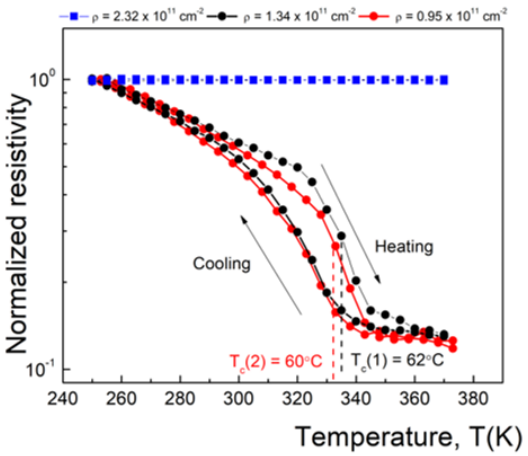

Fig. 5. Normalized resistivity-temperature curves on heating and cooling in the range of 250 – 370 K.

No variation of the resistance was seen in the case of the sample obtained at 400 °C. This could be explained considering the small intensity of the diffraction lines, in comparison with other two samples. According to the Rietveld data, this sample presents a small crystallite, accompanied by a higher lattice strain, which further implies a higher dislocation density. As the temperature increases to 500 °C, the decreasing of the resistance becomes visible, reaching to ~ 0.15. Also, for the sample with the lowest dislocation density, the normalized resistance decreased to ~ 0.10. At the same time, the hysteresis curve width became narrower in the presence of a smaller dislocation density. Also, it was showed that the resistance-temperatures are sluggish for poor crystalline quality, and the resistance drop becomes steeper at high quality of crystallinity [17].

3. Conclusions

These preliminary investigations in vanadium oxide films obtained by PLD at low oxygen pressure pointed out the possibility to obtain crystalline VO_2 thin films in a one-step process, starting from the ablation of a pure V_2O_5 target by PLD. The XRD results indicate that the unit cell parameters are not affected by the substrate temperature or number of pulses. On the other hand, the mean crystallite size, lattice strain or dislocation density are affected by the PLD growth parameters. At the same time, the optical properties, as well as the distribution of the vanadium oxidation state are modified. Corroborating the electrical measurements with the Rietveld refinement data, it was pointed out that the crystal quality plays a central role in the explaining of different features of resistance-temperature curves, such as the resistance drop or the hysteresis width.

Acknowledgements. This project has received funding from the European Union's Horizon 2020 research and innovation programme under grant agreement No 101007417 having benefitted from the access provided by ICN2 in Bellaterra, Barcelona within the framework of the NFFA-Europe Pilot Transnational Access Activity, proposal ID282. This research was partially financed by Romanian Core Program PNCDI 2022-2027 "Cercetari avansate in dispozitive micronano-electronice, fotonice, senzori si microsisteme pentru aplicatii societale- μNanoEl" cod 2307/29.12.2022 (2023-2026) and PN 23.21.01.06 project; financed by the Ministry of Research, Innovation and Digitalization. Also, this work was supported by a grant of the Ministry of Research, Innovation and Digitization, CCCDI - UEFISCDI, project number PN-III-P2-2.1-PED-2021-2688.

References

[1] K. LIU, S. LEE, S. YANG, O. DELAIRE and J. WU, *Recent progresses on physics and applications of vanadium dioxide*, Materials Today **21**(8), 2018, pp. 875–896.

[2] P. HU, P. HU, T. D. VU, M. LI, S. WANG, Y. KE, X. ZENG, L. MAI and Y. LONG, *Vanadium oxide: Phase diagrams, structures, synthesis, and applications*, Chemical Reviews **123**(8), 2023, pp. 4353–4415.

[3] N. HASSAN, J. RIAZ, M. T. QURESHI, A. RAZAQ, M. RAHIM, A. MUHAMMAD TOUFIQ and A. SHAKOOR, *Vanadium oxide (V_2O_3) for energy storage applications through hydrothermal route*, Journal of Materials Science: Materials in Electronics **29**(18), 2018, pp. 16021–16026.

[4] F. J. MORIN, *Oxides which show a metal-to-insulator transition at the neel temperature*, Physical Review Letters **3**(1), 1959, pp. 34–36.

[5] M. M. QAZILBASH, M. BREHM, B. G. CHAE, P. C. HO, G. O. ANDREEV, B. J. KIM, S. J. YUN, A. V. BALATSKY, M. B. MAPLE, F. KEILMANN, H. T. KIM and D. N. BASOV, *Mott transition in VO_2 revealed by infrared spectroscopy and nano-imaging*, Science **318**(5857), 2007, pp. 1750–1753.

[6] K. SCHNEIDER, *Optical properties and electronic structure of V_2O_5, V_2O_3 and VO_2*, Journal of Materials Science: Materials in Electronics **31**(13), 2020, pp. 10478–10488.

[7] L. RODRÍGUEZ, F. SANDIUMENGE, C. FRONTERA, J. M. CAICEDO, J. PADILLA, G. CATALÁN and J. SANTISO, *Strong strain gradients and phase coexistence at the metal-insulator transition in VO_2 epitaxial films*, Acta Materialia **220**, 2021, 2202021.

[8] O. OJELERE, D. GRAF, T. LUDWIG, N. VOGT, A. KLEIN and S. MATHUR, *Reductive transformation of V(iii) precursors into vanadium(ii) oxide nanowires*, Dalton Transactions **47**(19), 2018, pp. 6842–6849.

[9] Y. LIU, J. LIU, Y. LI, D. WANG, L. REN and K. ZOU, *Effect of annealing temperature on the structure and properties of titanium oxide films*, Optical Materials Express **6**(5), 2016, pp. 1552–1560.

[10] Y. Y. LUO, Q. ZHU, Y. X. ZHANG, S. S. PAN, S. C. XU, M. LIU and G. H. LI, *Optimization of microstructure and optical properties of VO_2 thin film prepared by reactive sputtering*, Journal of Applied Physics **113**, 2013, 183520.

[11] H. ZHANG, Z. WU, Q. HE and Y. JIANG, *Preparation and investigation of sputtered vanadium dioxide films with large phase-transition hysteresis loops*, Applied Surface Science **277**, 2013, pp. 218–222.

[12] Y. GOLTVYANSKYI, I. KHATSEVYCH, A. KUCHUK, V. KLADKO, V. MELNIK, P. LYTVYN, V. NIKIRIN and B. ROMANYUK, *Structural transformation and functional properties of vanadium oxide films after low-temperature annealing*, Thin Solid Films **564**, 2014, pp. 179–185.

[13] D. H. KIM and H. S. KWOK, *Pulsed laser deposition of VO_2 thin films*, Applied Physics Letters **65**(25), 1994, pp. 3188–3190.

[14] J. Y. SUH, R. LOPEZ, L. C. FELDMAN and R. F. HAGLUND, *Semiconductor to metal phase transition in the nucleation and growth of VO_2 nanoparticles and thin films*, Journal of Applied Physics **96**(2), 2004, pp. 1209–1213.

[15] N. ÉMOND, A, HENDAOUI, A. IBRAHIM, I. AL-NAIB, T. OZAKI and M. CHAKER, *Transmission of reactive pulsed laser deposited VO_2 films in the THz domain*, Applied Surface Science **379**, 2016, pp. 377–383.

[16] E.K. KOUSSI, F. BOURQUARD, T. TITE, D. JAMON, F. GARRELIE and Y.JOURLIN, *Synthesis of vanadium oxides by pulsed laser deposition and rapid thermal annealing*, Applied Surface Science **521**, 2020, 146267.

[17] S. A. BUKHARI, S. KUMAR, P. KUMAR, S. P. GUMFEKAR, H. J. CHUNG, T. THUNDAT and A. GOSWAMI, *The effect of oxygen flow rate on metal–insulator transition (MIT) characteristics of vanadium dioxide (VO_2) thin films by pulsed laser deposition (PLD)*, Applied Surface Science **529**, 2020, 146995.

[18] D. DIJKKAMP, T. VENKATESAN, X. D. WU, S. A. SHAHEEN, N. JISRAWI, Y. H. MIN-LEE, W. L. MCLEAN and M. CROFT, *Preparation of Y-Ba-Cu oxide superconductor thin films using pulsed laser evaporation from high Tc bulk material*, Applied Physics Letters **51**(8), 1987, pp. 619–621.

[19] J. NARAYAN and V. M. BHOSLE, *Phase transition and critical issues in structure-property correlations of vanadium oxide*, Journal of Applied Physics **100**(10), 2006, 103524.

[20] A. MOATTI, R. SACHAN, V. R. COOPER and J. NARAYAN, *Electrical Transition in Isostructural VO_2 Thin-Film Heterostructures*, Scientific Reports **9**(1), 2019, pp. 1–10.

[21] C. ROMANITAN, J. M. CAICEDO, I. MIHALACHE, J. PADILLA-PANTOJA and R. GAVRILA, *Synthesis of Vanadium dioxide by pulsed laser deposition using a one-dtep process*, Proceedings of 2023 International Semiconductor Conference, Sinaia, Romania, 2023, pp. 21–24.

[22] C. A. SCHNEIDER, W. S. RASBAND and K. W. ELICEIRI, *NIH Image to ImageJ: 25 years of image analysis*, Nature Methods **9**(7), 2012, pp. 671–675.

[23] J. DAILLANT and A. GIBAUD, *X-ray and Neuron Reflectivity: Principles and Applications*, Springer-Verlag, Heidelberg, 1999.

[24] M. BIRKHOLZ, P.F. FEWSTER and C. GENZEL, *Thin Film Analysis by X-Ray Scattering*, Wiley-VCH Verlag, Weinheim, 2006.

[25] H. M. RIETVELD, *A profile refinement method for nuclear and magnetic structures*, Journal of Applied Crystallography **2**(2), 1969, pp. 65–71.

[26] A. D. FRENCH, *Increment in evolution of cellulose crystallinity analysis*, Cellulose **27**(10), 2020, pp. 5445–5448.

[27] G. K. WILLIAMSON and R. E. SMALLMAN, *III. Dislocation densities in some annealed and cold-worked metals from measurements on the X-ray Debye-Scherrer spectrum*, Philosophical Magazine **1**(1), 1956, pp. 34–46.

[28] C. LAMSAL and N. M. RAVINDRA, *Optical properties of vanadium oxides-an analysis*, Journal of Materials Science **48**(18), 2013, pp. 6341–6351.

[29] H. T. FAN, X. M. TENG, S. S. PAN, C. YE, G. H. LI and L. D. ZHANG, O*ptical properties of δ-Bi2 O3 thin films grown by reactive sputtering*, Applied Physics Letters **87**(23), 2005, pp. 1–3.

[30] R. GHOSH, D. BASAK and S. FUJIHARA, *Effect of substrate-induced strain on the structural, electrical, and optical properties of polycrystalline ZnO thin films*, Journal of Applied Physics **96**(5), 2004, pp. 2689–2692.

[31] J. TAUC, R. GRIGOROVICI and A. VANCU, *Optical properties and electronic structure of amorphous Germanium*, Physica Status Solidi (A): Applications and Materials Science **15**, 1966, pp. 627–637.

[32] S. LEE, T. L. MEYER, C. SOHN, D. LEE, J. NICHOLS, D. LEE, S. S. A. SEO, J. W. FREELAND, T. W. NOH and H. N. LEE, *Electronic structure and insulating gap in epitaxial VO_2 polymorphs*, APL Materials **3**(12), 2015, 126109.

[33] G. SILVERSMIT, H. POELMAN and R. DE GRYSE, *Influence of magnetron deposition parameters on the stoichiometry of sputtered VO_2O_5 films*, Surface and Interface Analysis **36**(8), 2004, pp. 1163–1166.